Supporting Information:

Effects of Fluorination and Side Chain Branching on Molecular Conformation and Photovoltaic Performance of Donor-Acceptor Copolymers

Sebastian Wood,[†] Ji-Hoon Kim,[§] Do-Hoon Hwang,[§] Ji-Seon Kim[†,*]

[†]Department of Physics and Centre for Plastic Electronics, Imperial College London, London, SW7 2AZ, United Kingdom

[§]Department of Chemistry, and Chemistry Institute for Functional Materials, Pusan National University, Busan 609-735, Republic of Korea

*Corresponding Author. Email: ji-seon.kim@imperial.ac.uk

Syntheses of A-PBDTBTz and F-PBDTBTz

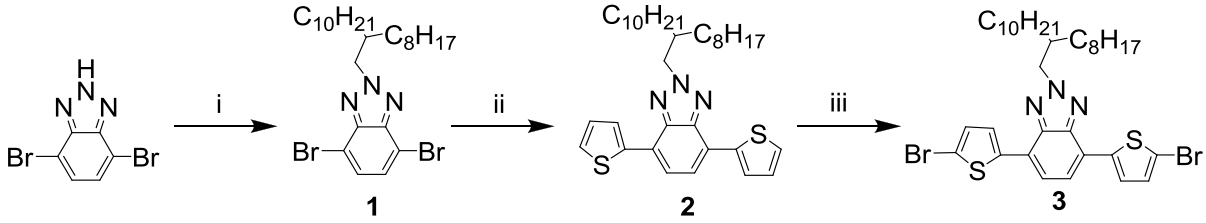

Scheme S1. i) THF, 2-octyl-1-dodecanol, diisopropyl azodicarboxylate (DIAD), triphenylphosphine (PPh_3), 0 °C, overnight, ii) Tripropyl(thiophen-2-yl)stannane, $PdCl_2(PPh_3)_2$, DMF, reflux, overnight, iii) N-bromosuccinimide (NBS), DMF, overnight.

Synthesis of 4,7-dibromo-2-(2-octyldodecyl)-2H-benzo[d][1,2,3]triazole (1). To a magnetically stirred solution of 4,7-dibromo-2H-benzo[d][1,2,3]triazole (2.0 g, 7.2 mmol), 2-octyl-1-dodecanol (3.23 g, 10.8 mmol) and triphenyl phosphine (2.84 g, 10.8 mmol) in THF (50 mL) was added diisopropyl azodicarboxylate (2.77 g, 10.8 mmol) at 0 °C under a N2 atmosphere. After stirring for 3 h, the reaction mixture was poured into H_2O (200 mL), and the product was extracted with diethyl ether. The organic layer was washed with brine, dried over anhydrous $MgSO_4$, and concentrated under reduced pressure. The crude product was purified by column chromatography and then crystallized from an isopropanol/hexane mixture to give compound 1 as colorless crystals (2.11 g, 50%) ^{1}H NMR (300 MHz, $CDCl_3$) δ: 7.45 (s, 2H), 4.75 (d, 2H), 2.25 (m, 1H), 1.36 (m, 24H), 1.24 (br, 64H), 0.85 (m, 12H). Anal. Calcd. for $C_{26}H_{43}Br_2N_3$: C, 56.02; H, 7.77; Br, 28.67; N, 7.54. Found: C, 55.81; H, 7.80; N, 7.46.

Synthesis of 2-(2-octyldodecyl)-4,7-di(thiophen-2-yl)-2H-benzo[d][1,2,3]triazole (2). Tripropyl(thiophen-2-yl)stannane (1.67 g, 4.4 mmol) was added to a stirred solution of 4,7-dibromo-2-(2-octyldodecyl)-2H-benzo[d][1,2,3]triazole (1.00 g, 1.77 mmol), and bis(triphenylphosphine)palladium(II) dichloride (95 mg, 0.06 mmol) in DMF (50 mL). The mixture was refluxed overnight, and then extracted with ethyl acetate. The organic layer was washed with $NaHCO_3$ and brine, and then dried over anhydrous $MgSO_4$. The solvent was removed and the crude product was purified using column chromatography on silica with hexane as eluent, to yield 2 (1.5 g, 58%) as pale yellow solid. ^{1}H NMR (300 MHz, $CDCl_3$) δ: 8.10 (d, 2H), 7.62 (s, 2H), 7.28 (d, 2H), 7.18 (t, 2H), 4.75 (d, 2H), 2.19 (m, 1H), 1.39 (m, 24H), 1.23 (br, 64H), 0.86 (m, 12H). Anal. Calcd. for $C_{34}H_{49}N_3S_2$: C, 72.42; H, 8.76; N, 7.45; S, 11.37. Found: C, 71.95; H, 8.80; N, 7.39; S, 11.12.

Synthesis of 4,7-bis(5-bromothiophen-2-yl)-2-(2-octyldodecyl)-2H-benzo[d][1,2,3]triazole (3). N-Bromosuccinimide (0.78 g, 4.42 mmol) was added to a stirred solution of compound 2 (1.00 g, 1.77 mmol) in DMF (25 mL) in the absence of light. The mixture was stirred at room temperature for 4 h, and a bright yellow solid precipitate was formed. The mixture was filtered and washed thoroughly with methanol. The solid was then washed once with cold diethyl ether and purified by flash chromatography to give 3 (1.20 g, 80%). ^{1}H NMR (300 MHz, $CDCl_3$) δ: 8.15 (d, 2H), 7.54 (s, 2H), 7.17 (d, 2H), 4.77 (d, 2H), 2.23 (m, 1H), 1.40 (m, 24H), 1.21 (br, 64H), 0.85 (m, 12H). Anal. Calcd. for $C_{34}H_{47}Br_2N_3S_2$: C, 56.58; H, 6.56; N, 5.82; S, 8.89. Found: C, 56.21; H, 6.60; N, 5.75; S, 8.60.

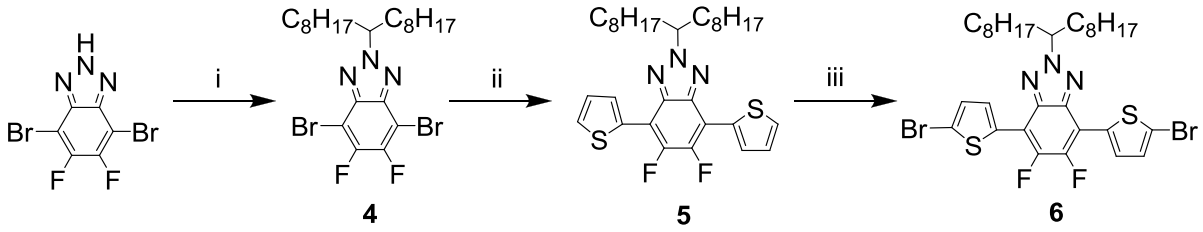

4 **5** **6**

Scheme S2. i) THF, heptadecan-9-ol, diisopropyl azodicarboxylate (DIAD), triphenylphosphine (PPh_3), 0 °C, overnight, ii) Tripropyl(thiophen-2-yl)stannane, $PdCl_2(PPh_3)_2$, DMF, reflux, overnight, iii) N-bromosuccinimide (NBS), THF, overnight.

Synthesis of 4,7-dibromo-5,6-difluoro-2-(heptadecan-9-yl)-2H-benzo[d][1,2,3]triazole (4). Diisopropyl azodicarboxylate (0.77 g, 4.78 mmol) was added to a magnetically stirred solution of 4,7-dibromo-5,6-difluoro-2H-benzo[d][1,2,3]triazole (1.00 g, 3.19 mmol), heptadecan-9-ol (1.00 g, 4.78 mmol), and triphenyl phosphine (1.00 g, 4.78 mmol) in tetrahydrofuran (50 mL) at 0 °C under nitrogen. After stirring for 3 h, the reaction mixture was poured into water (200 mL), and the product was extracted with diethyl ether. The organic layer was washed with brine, dried over anhydrous $MgSO_4$, and concentrated under reduced pressure. The crude product was purified by column chromatography and then crystallized from an isopropanol/hexane mixture to give compound 2 as colorless crystals (1.10 g, 50% yield). ^{1}H NMR (300 MHz, $CDCl_3$, δ): 7.44 (s, 2H), 4.90 (m, 1H), 2.35 (m, 2H), 2.01 (m, 2H), 1.31–1.21 (m, 22H), 1.08–0.96 (m, 2H), 0.86 (t, 6H). Anal. Calcd. for $C_{23}H_{37}Br_2N_3$: C, 53.60; H, 7.24; Br, 31.01; N, 8.15; found: C, 53.80; H, 7.30; N, 8.10.

Synthesis of 5,6-difluoro-2-(heptadecan-9-yl)-4,7-di(thiophen-2-yl)-2H-benzo[d][1,2,3]triazole (5). Tripropyl(thiophen-2-yl)stannane (4.50 g, 13.6 mmol) was added to a stirred solution of 4 (3.00 g, 5.44 mmol) and bis(triphenylphosphine)palladium(II)dichloride (0.13 g, 0.06 mmol) in DMF (50 mL). The mixture was refluxed overnight, and then extracted with ethyl acetate. The organic layer was washed with $NaHCO_3$ and brine, and then dried over anhydrous $MgSO_4$. The solvent was removed and the crude product was purified using column chromatography on silica with hexane as the eluent, to yield 5 (3.3 g, 58% yield) as a pale-yellow solid. ^{1}H NMR (300 MHz, $CDCl_3$, δ): 8.05 (d, 2H), 7.65 (s, 2H), 7.31 (d, 2H), 7.23 (t, 2H), 4.90 (m, 1H), 2.35 (m, 2H), 2.01 (m, 2H), 1.31–1.21 (m, 22H), 1.08–0.96 (m, 2H), 0.86 (t, 6H). Anal. Calcd. for $C_{31}H_{43}N_3S_2$: C, 71.35; H, 8.31; N, 8.05; S, 12.29; found: C, 70.88; H, 8.25; N, 7.98; S, 12.11.

Synthesis of 4,7-bis(5-bromothiophen-2-yl)-5,6-difluoro-2-(heptadecan-9-yl)-2H-benzo[d][1,2,3]triazole (6). N-Bromosuccinimide (0.7 g, 4.48 mmol) was added to a stirred solution of 5 (1.00 g, 1.79 mmol) in tetrahydrofuran (25 mL) in the absence of light. The mixture was stirred at room temperature for 4 h, and a bright-yellow solid precipitate formed. The mixture was filtered and washed thoroughly with methanol. The solid was then washed once with cold diethyl ether and purified by flash chromatography to give 6 (1.50 g, 71% yield).^{1}H NMR (300 MHz, CDCl3, δ): 7.81 (d, 2H), 7.50 (s, 2H), 7.11 (d, 2H), 4.90 (m, 1H), 2.35 (m, 2H), 2.01 (m, 2H), 1.31–1.21 (m, 22H), 1.08–0.96 (m, 2H), 0.86 (t, 6H). Anal. Calcd. for $C_{31}H_{41}Br_2N_3S_2$: C, 54.79; H, 6.08; N, 6.18; S, 9.44; found: C, 55.01; H, 6.00; N, 5.99; S, 8.74.

General Polymerization Procedure. All polymers were synthesized using Stille cross-coupling. A solution of the monomers and tetrakis(triphenylphosphine)palladium in anhydrous toluene (4 mL) and dimethylformamide (DMF; 1 mL) was stirred at 120 °C for 2 days. 2-Bromothiophene and tripropyl(thiophen-2-yl)stannane end-cappers dissolved in anhydrous toluene (1 mL) were added and the mixture was stirred for an additional 12 h. The mixture was then cooled to ~50 °C and poured into methanol (200 mL), with vigorous stirring. The resulting polymer fibers were collected by filtration and further purified by washing with acetone for 2 days in a Soxhlet apparatus to remove any oligomer remnants and catalyst residues, followed by silica gel column chromatography, using chloroform as the eluent. The resulting polymer was soluble in common organic solvents.

Density Functional Theory Geometry Optimization

In order to interpret the Raman spectra, density functional theory with GAUSSIAN09 software[1] was first used to optimize the geometry (B3LYP 6-311G*)[2–4] of a symmetric segment of the polymer backbone (Donor-Acceptor-Donor-Acceptor-Donor with thiophene end groups), using truncated alkyl chains. Both PBDTBTz (corresponding with both S-PBDTBTz and A-PBDTBTz) and F-PBDTBTz were modelled in this way and the main differences in geometry are summarized in Table S1.

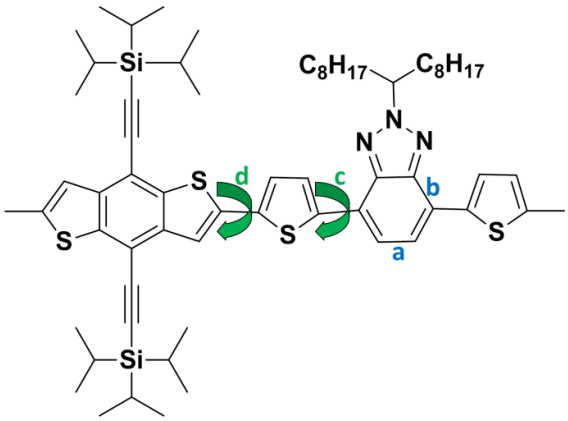

Figure S1. Schematic diagram of a S-PBDTBTz unit identifying bonds which show variation in DFT optimized geometry due to fluorination of benzotriazole unit.

Table S1. Bond lengths and inter-unit dihedral angles showing variation in DFT optimized geometries for PBDTBTz (S-PBDTBTz or A-PBDTBTz) and F-PBDTBTz backbone segments. See Figure 7 for bond identification.

	S/A-PBDTBTz	F-PBDTBTz
a - bond length (Å)	1.408	1.414
b - bond length (Å)	1.431	1.436
c – dihedral (°)	1.4	0.5
d – dihedral (°)	9.3	11.6

Vibrational Mode Assignments

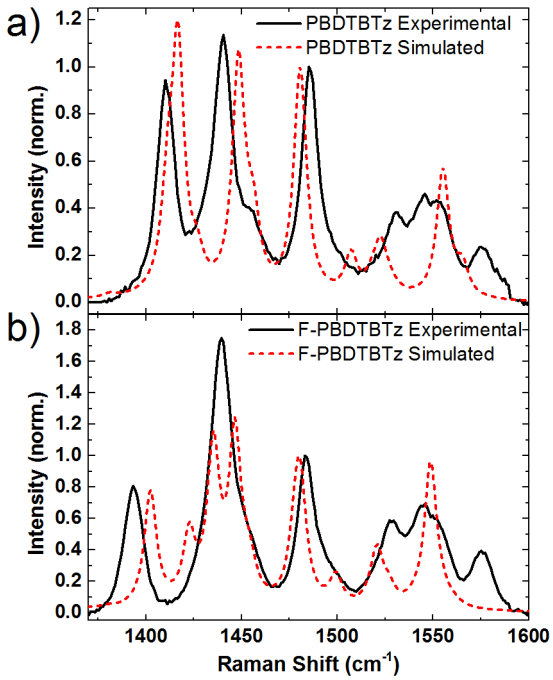

Figure S2. Comparison of simulated and experimental Raman spectra (785 nm excitation) for, a) PBDTBTz (S-PBDTBTz and A-PBDTBTz), and b) F-PBDTBTz.

Vibrational modes were calculated based on the optimized geometry and the resulting simulated Raman spectra are given in Figure S2 alongside experimental spectra measured under 785 nm excitation. The simulated and experimental spectra correspond well for the peaks measured at 1410 (1393 in F-PBDTBTz), 1440, 1454, 1485 and 1531 cm^{-1} enabling these modes to be readily identified. The 1546, 1552 and 1575 cm^{-1} mode energies are not well reproduced by the model and all have modelled energies close to 1560 cm^{-1}, however, the 1546 and 1552 cm^{-1} modes have been identified previously and correspond closely to the modes of the better-known benzothiadiazole unit.[5] The remaining benzodithiophene ring stretching mode is assigned to the 1575 cm^{-1} peak, and this interpretation is found to be consistent with the results discussed here. These vibrational mode assignments are illustrated by Figure S3 indicating the main bond stretches involved in each mode.

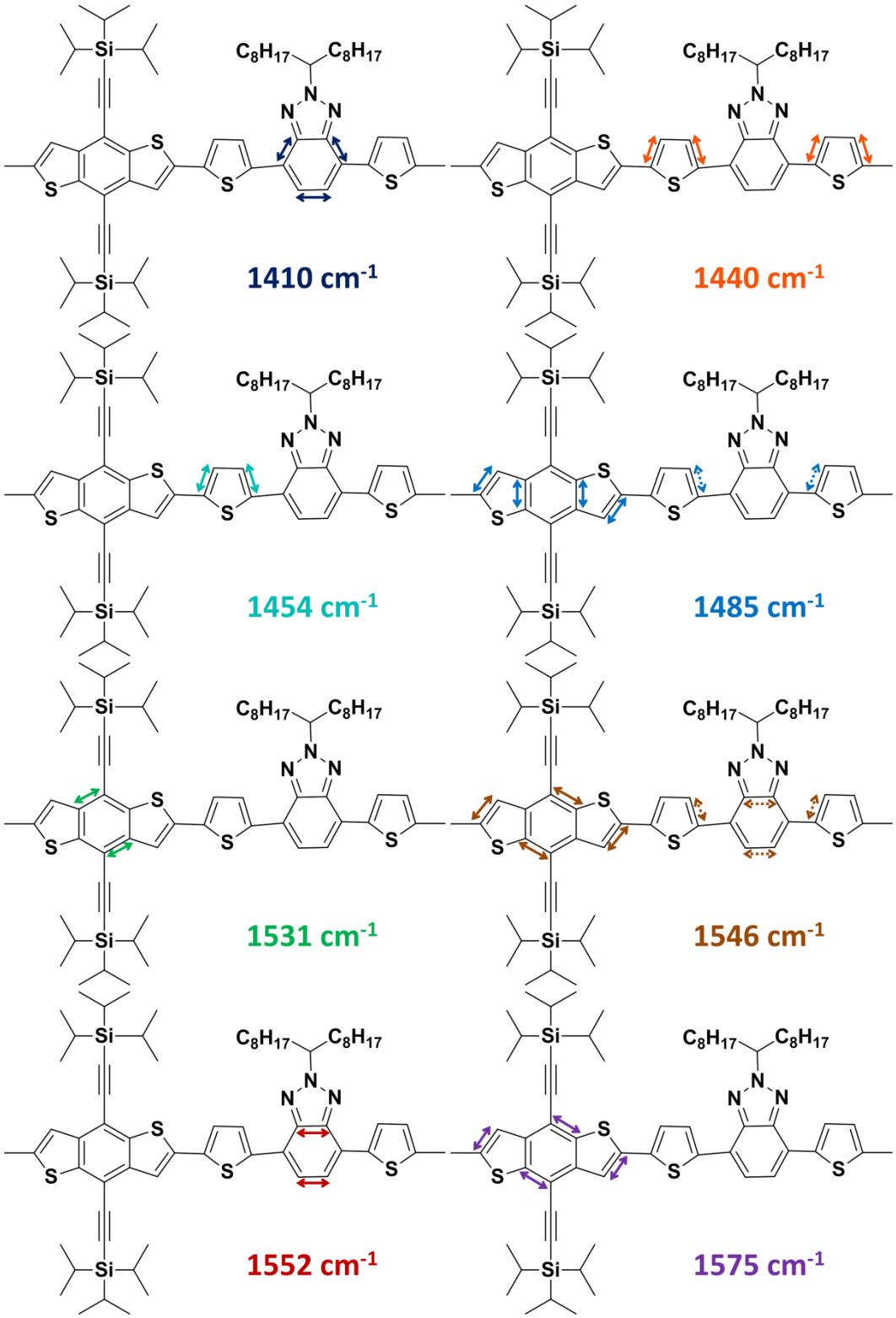

Figure S3. Diagram indicating the main bond stretch assignments for Raman-active vibrational modes at 1410, 1440, 1454, 1485, 1531, 1546, 1552, and 1575 cm^{-1} (peak position values taken from S-PBDTBTz spectrum). Dotted arrows indicate weaker contributions.

Raman Spectrum Peak Fitting

Raman peak intensities are extracted from the measured spectra by peak fitting with a series of Lorentzian peaks with fixed width (12.5 cm^{-1}) and fixed positions (± 1 cm^{-1}) except for the 1410/1393 cm^{-1} peak in F-PBDTBTz. The result of this fitting is shown in Figure S4, and, although the quality of fitting is poorer at lower wavenumbers, we consider it satisfactory for our purposes.

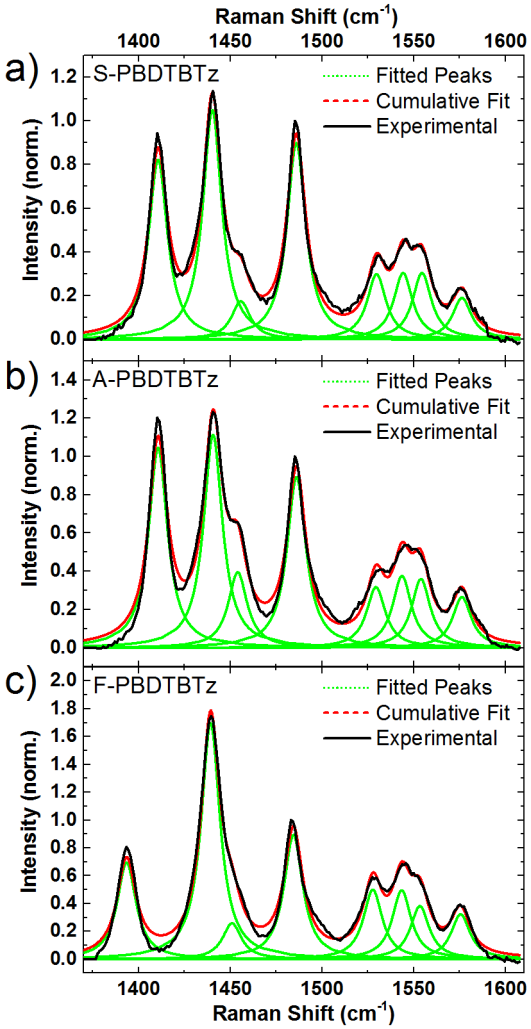

Figure S4. Peak fitting to non-resonant Raman spectra (785 nm excitation) with Lorentzian peaks for neat polymer thin films comparing: a) S-PBDTBTz, b) A-PBDTBTz, and c) F-PBDTBTz. Normalized to peak at 1485 cm^{-1}.

Interunit Dihedral Torsion

The effects of the different interunit dihedral angles on the Raman spectra were considered by enforcing a range of torsional angles from 0° to 40° as a frozen coordinate and then calculating Raman activity for optimized molecular geometries. Figure S4 shows these results considering first the case where the BDT unit is twisted out of the molecular backbone plane (BDT-T torsion), and second the corresponding situation with the BTz unit twisted (BTz-T torsion). The signs of the bond angles alternate so that the molecular backbone planarity is otherwise conserved (as opposed to the helical case).

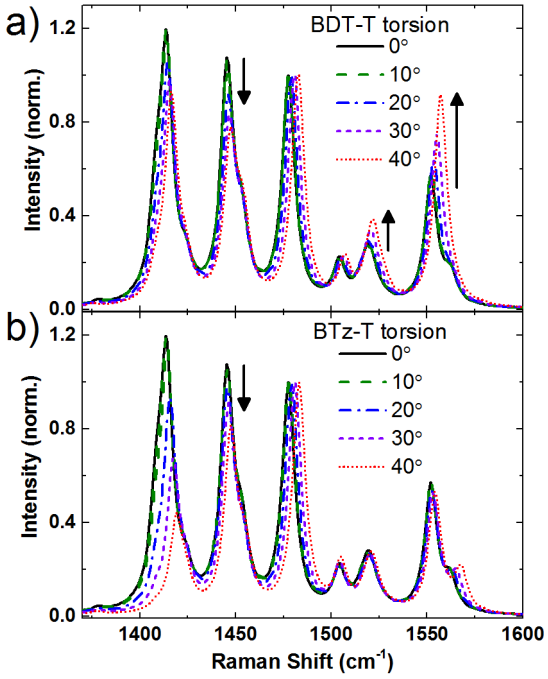

Figure S5. Calculated Raman spectra for PBDTBTz showing the effect of dihedral torsion applied to, a) BDT-T bond, and b) BTz-T bond, normalized to the 1485 cm^{-1} peak.

The calculated spectra are normalized to the fused thiophene C=C mode around 1485 cm^{-1} for comparison with the measured spectra shown throughout this work. These calculations only consider the non-fluorinated case and since fluorination of the BTz unit will significantly affect those modes, we restrict ourselves to discussion of modes localised on the BDT and T units. In both cases (BDT-T and BTz-T torsion) we find that the relative intensity of the thiophene peak (around 1450 cm^{-1}) decreases with torsion so this does not enable us to distinguish between the two cases. However, the BDT-T torsion also shows an increase in the relative intensity of a peak at 1520 cm^{-1} which we identify as the BDT ring stretch

measured at 1531 cm^{-1} – this is not observed in the BTz-T torsion so identifies the ratio I_{1485}/I_{1531} as a measure of BDT-T torsion (higher value corresponding to greater BDT-T planarity). We see a similar increase in the intensity of the mode calculated around 1560 cm^{-1}. The overlapping modes in this region here are hard to distinguish but this might be identified as the peak measured at 1575 cm^{-1} and so suggests I_{1485}/I_{1575} as another indicator of BDT-T torsion. Similarly the differences in intensities of the 1546 and 1552 cm^{-1} modes are not visibly distinct in these calculated spectra because of overlapping peaks but a similar argument applies based on the quenching of the more delocalized mode (1546 cm^{-1}) due to BTz-T torsion, observed in our previous work.[5] The ratio I_{1546}/I_{1552} is therefore considered a good measure of BTz-T torsion and the conclusions are consistent with geometry optimization calculations and the other results presented in this work.

Resonant Raman Spectroscopy

In donor-acceptor type copolymers we commonly measure two strong absorption bands, often described as 'charge-transfer' and 'π-π*' transitions based on the localization of the calculated molecular orbitals. Resonant Raman spectroscopy offers an experimental tool to probe the changes in the (de)localization of molecular orbitals resulting from optical absorptions at different wavelengths. In this case the donor-acceptor polymers show one very strong main absorption band (450-630 nm) and a smaller absorption feature peaking around 400 nm (see Figure 2). Resonant Raman is used here to identify the nature of the optical absorption transitions represented within the main, lower energy band.

Figure S6 shows the resonant Raman spectra of these polymers under a range of excitation wavelengths spread across the absorption band (457, 488, 514, and 633 nm) as well as the non-resonant case (785 nm). The resonant enhancement in the relative intensities of particular modes gives an indication of how the electronic absorption transitions are localized on particular units within the molecule. Specifically, the resonant enhancement is greatest for the vibrational modes corresponding most strongly with the geometry distortion caused by the electronic transition to the Franck-Condon excited state.[6]

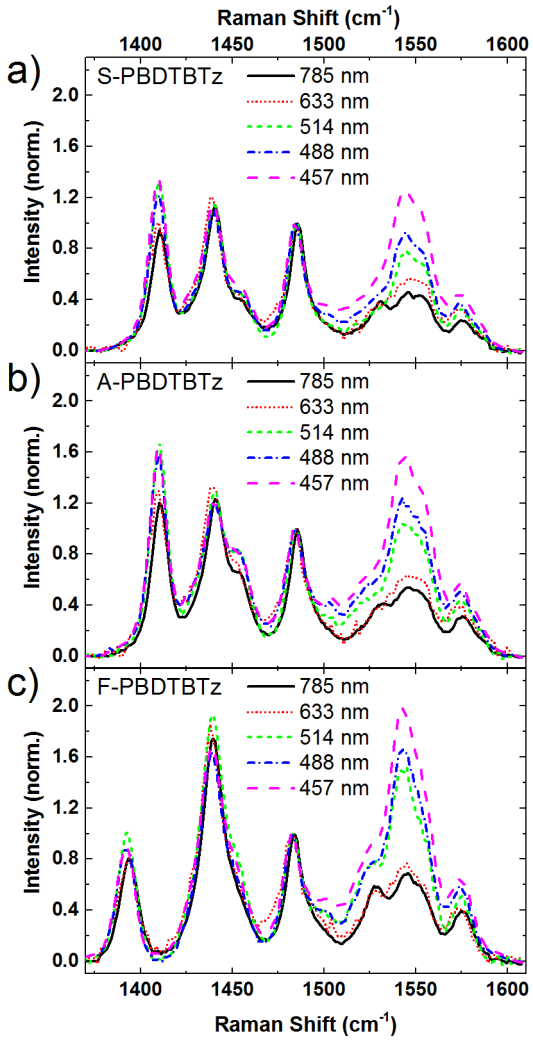

Figure S6. Resonant Raman spectra for neat polymer thin films comparing spectra measured under 785, 633, 514, 488 and 457 nm excitation for, a) S-PBDTBTz, b) A- PBDTBTz, and c) F-PBDTBTz. Normalized to peak at 1485 cm^{-1}.

All three polymers show a strong resonant enhancement of the 1546 and 1552 cm^{-1} modes relative to the 1485 cm^{-1} mode which is weak for 633 nm excitation but increases as the excitation wavelength moves further into the absorption band, giving a maximum enhancement with 457 nm excitation. Since these enhanced modes both have strong contributions from the benzotriazole unit ring stretch, this is clear evidence that the electronic transitions in this absorption band are coupled to distortions of the bonds in the benzotriazole ring suggesting that the excitations have significant charge transfer character. There is also a smaller corresponding enhancement of the 1410 (1393 in F-PBDTBTz) cm^{-1} mode, which is also localized on the benzotriazole unit. This resonant enhancement of benzodithiophene modes is strongest for the excitations close to the high energy edge of

the main absorption band (maximum for 457nm) but minimal for excitation at the low energy absorption onset (633 nm). This indicates that within the main absorption band, the higher energy part couples more strongly with the vibrational modes localized on the ring of the acceptor unit. It is, however, not possible to distinguish whether this results from the presence of multiple different electronic transitions, different conformational phases in the film, or if the shorter wavelengths simply couple more strongly to the benzotriazole ring stretch vibrational modes.

2D Grazing Incidence X-ray Diffraction Line-Cuts

Figure S7 shows X-ray scattering intensity line-cuts along the in-plane (xy) and out-of-plane (z) directions on the 2D plots shown in the manuscript.

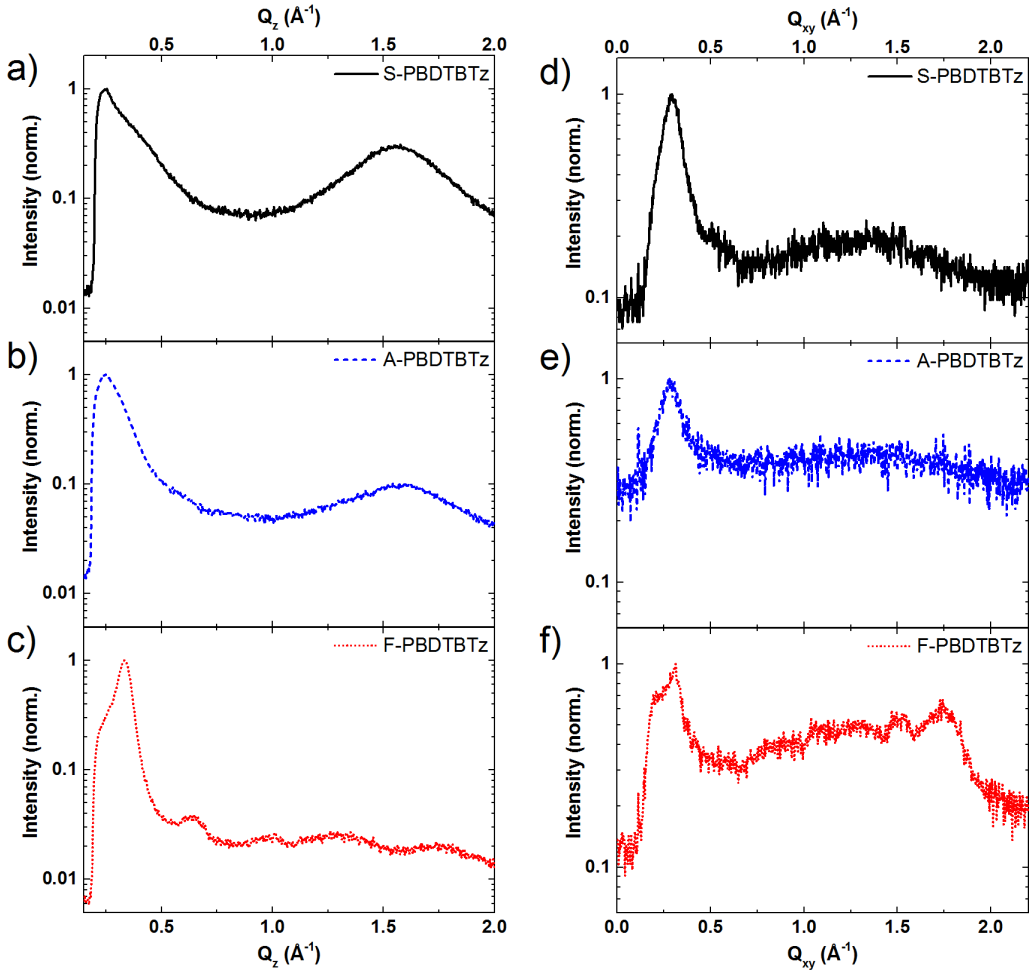

Figure S7. X-ray diffraction line-cuts taken from 2D data shown in manuscript for S-PBDTBTz, A-PBDTBTz, and F-PBDTBTz, along the z-direction (a-c), and along the xy direction (d-f).

Thin Film Transistors

Transfer characteristics of A-PBDTBTz and F-PBDTBTz transistors are given in Figure S8. Equivalent data for S-PBDTBTz measured in the same experiment have been published previously.[5]

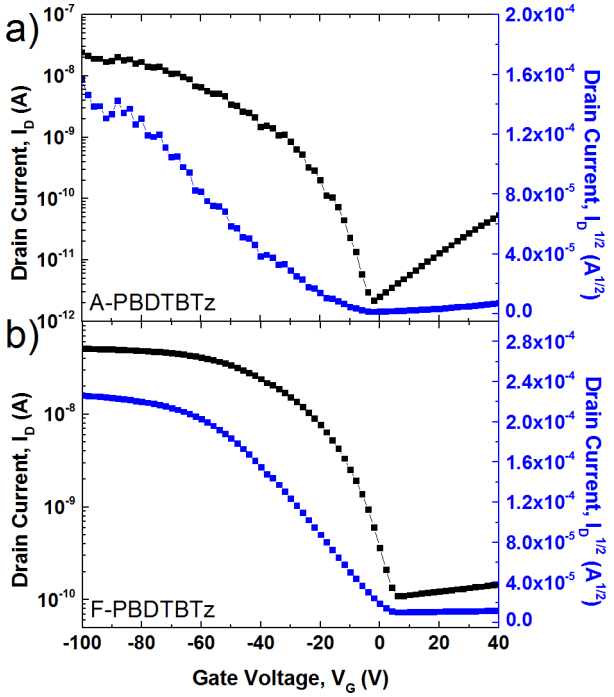

Figure S8. Transfer characteristics with 80 V source-drain bias for transistor devices fabricated from thin films of, a) A-PBDTBTz, and b) F-PBDTBTz.

Photovoltaic Device Performance

Current-voltage characteristics of A-PBDTBTz and F-PBDTBTz (polymer:$PC_{71}BM$ blends with and without DIO additive) photovoltaic devices are given in Figure S9. Equivalent data for S-PBDTBTz measured in the same experiment have been published previously.[5]

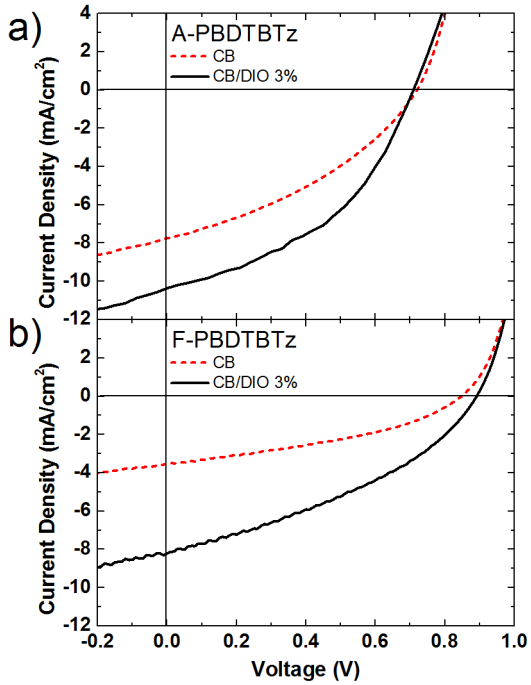

Figure S9. Current-voltage characteristics for polymer:$PC_{71}BM$ blend film photovoltaic devices measured under AM 1.5 G illumination with 100 mW/cm^2 intensity for, a) A-PBDTBTz, and b) F-PBDTBTz, with and without DIO additive.

External Quantum Efficiency (EQE) spectra for the optimized photovoltaic devices (with and without the DIO additive) are shown in Figure S10.

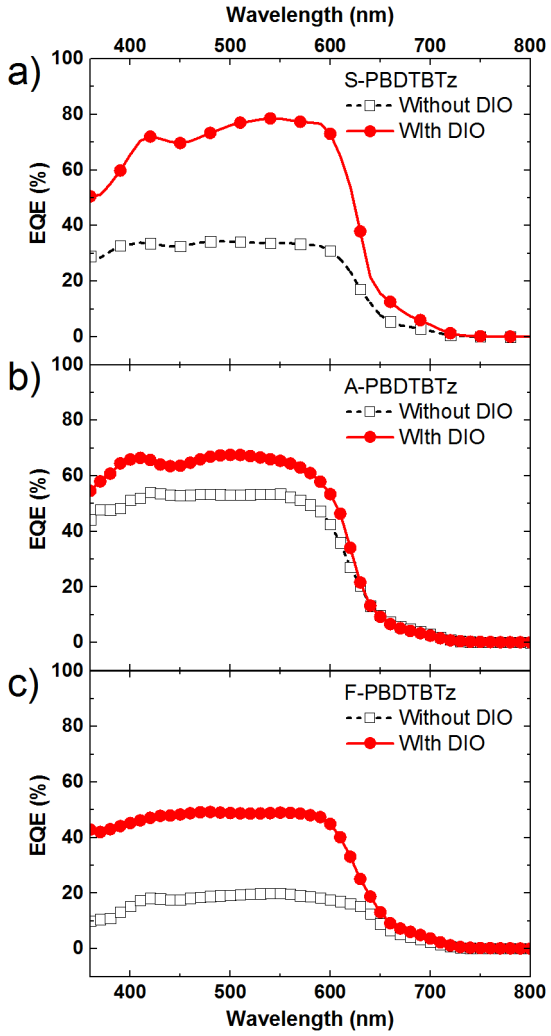

Figure S10. EQE spectra measured for optimized photovoltaic devices made with and without DIO, for a) S-PBDTBTz, b) A-PBDTBTz, and c) F-PBDTBTz.

References

(1) Frisch, M. J.; Trucks, G. W.; Schlegel, H. B.; Scuseria, G. E.; Robb, M. A.; Cheeseman, J. R.; Scalmani, G.; Barone, V.; Mennucci, B.; Petersson, G. A.; Nakatsuji, H.; Caricato, M.; Li, X.; Hratchian, H. P.; Izmaylov, A. F.; Bloino, J.; Zheng, G.; Sonnenberg, J. L.; Hada, M.; Ehara, M.; Toyota, K.; Fukuda, R.; Hasegawa, J.; Ishida, M.; Nakajima, T.; Honda, Y.; Kitao, O.; Nakai, H.; Vreven, T.; Montgomery, Jr., J. A.; Peralta, J. E.; Ogliaro, F.; Bearpark, M.; Heyd, J. J.; Brothers, E.; Kudin, K. N.; Staroverov, V. N.; Kobayashi, R.; Normand, J.; Raghavachari, K.; Rendell, A.; Burant, J. C.; Iyengar, S. S.; Tomasi, J.; Cossi, M.; Rega, N.; Millam, J. M.; Klene, M.; Knox, J. E.; Cross, J. B.;

Bakken, V.; Adamo, C.; Jaramillo, J.; Gomperts, R.; Stratmann, R. E.; Yazyev, O.; Austin, A. J.; Cammi, R.; Pomelli, C.; Ochterski, J. W.; Martin, R. L.; Morokuma, K.; Zakrzewski, V. G.; Voth, G. A.; Salvador, P.; Dannenberg, J. J.; Dapprich, S.; Daniels, A. D.; Farkas, Ö.; Foresman, J. B.; Ortiz, J. V.; Cioslowski, J.; Fox, D. J. Gaussian 09, Revision A.1, 2009.

(2) Becke, A. D. Density-functional thermochemistry. III. The role of exact exchange. *J. Chem. Phys.* **1993**, *98*, 5648-5652.

(3) McLean, A. D.; Chandler, G. S. Contracted Gaussian basis sets for molecular calculations. I. Second row atoms, Z=11–18. *J. Chem. Phys.* **1980**, *72*, 5639-5648.

(4) McGrath, M. P.; Radom, L. Extension of Gaussian-1 (G1) theory to bromine-containing molecules. *J. Chem. Phys.* **1991**, *94*, 511-516.

(5) Kim, J.-H.; Song, C. E.; Shin, N.; Kang, H.; Wood, S.; Kang, I.; Kim, B. J.; Kim, B.; Kim, J.; Shin, W. S.; Hwang, D. High-Crystalline Medium-Band-Gap Polymers Consisting of Benzodithiophene and Benzotriazole Derivatives for Organic Photovoltaic Cells. *ACS Appl. Mater. Interfaces* **2013**, 5, 12820-12831.

(6) Myers, A. B. Resonance Raman Intensities and Charge-Transfer Reorganization Energies. *Chem. Rev.* **1996**, *96*, 911-926.